

# Ab Initio Study of the H + HONO Reaction: Direct Abstraction versus Indirect Exchange Processes

C.-C. Hsu, M. C. Lin,\* and A. M. Mebel†

Department of Chemistry, Emory University, Atlanta, Georgia 30322

C. F. Melius

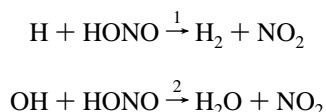
Combustion Research Facility, Sandia National Laboratories, Livermore, California 94552

Received: July 29, 1996; In Final Form: September 30, 1996<sup>®</sup>

The mechanism of the H + HONO reaction (for which no experimental data are available) has been elucidated by ab initio molecular orbital calculations using modified G2 and BAC-MP4 methods. These results indicate that the reaction occurs predominantly by two indirect metathetical processes. One produces OH + HNO and H<sub>2</sub>O + NO from the decomposition of vibrationally excited hydroxyl nitroxide, HN(O)OH, formed by H atom addition to the N atom of HONO. The other produces H<sub>2</sub>O + NO from the decomposition of vibrationally excited dihydroxylamino radical, N(OH)<sub>2</sub>, formed by H atom addition to the terminal O atom. These indirect displacement processes are much more efficient than the commonly assumed, direct H-abstraction reaction producing H<sub>2</sub> + NO<sub>2</sub>. A transition-state theory calculation for the direct abstraction reaction and RRKM calculations for the two indirect displacement processes give rise to the following rate constants, in units of cm<sup>3</sup> molecule<sup>-1</sup> s<sup>-1</sup> for the 300–3500 K temperature range under atmospheric conditions:  $k_{\text{H}_2} = 3.33 \times 10^{-16} T^{1.55} \exp(-3328.5/T)$ ,  $k_{\text{OH}} = 9.36 \times 10^{-14} T^{0.86} \exp(-2500.8/T)$ ,  $k_{\text{H}_2\text{O}} = 1.35 \times 10^{-17} T^{1.89} \exp(-1935.7/T)$ , where the rate constant for H<sub>2</sub>O production represents the sum from both indirect displacement reactions.

## Introduction

Nitrous acid (HONO) plays a key role in the combustion of energetic materials such as nitramines and nitrate esters.<sup>1</sup> It is also a potential product of NO<sub>2</sub> reactions with alkoxy and peroxyalkyl radicals, which may occur in tropospheres.<sup>2</sup> Because of its weak O–H bond,  $D(\text{ONO}-\text{H}) = 78.3 \pm 0.5$  kcal/mol,<sup>3</sup> HONO may be an efficient free radical scavenger under deNO<sub>x</sub> and propellant combustion conditions, for example<sup>4</sup>



In this work, we investigated the mechanism for the reaction of H atoms with HONO, the simplest case of the R<sup>•</sup> + HONO reactions (for which no experimental data are available<sup>4</sup>), using two variations of the Gaussian-2 (G2) ab initio molecular orbital calculation method recently developed by Pople and co-workers<sup>5</sup> to search for all possible reaction pathways. The results of these calculations are compared with those obtained by the bond-additivity-corrected fourth-order perturbation Møller–Plesset (BAC-MP4) technique.<sup>6</sup>

The results of this comprehensive study reveal that the commonly assumed direct abstraction reaction (1) is a minor process and that the indirect metathetical reactions taking place by H atom addition to the N atom as well as to the terminal O atom, producing HNO + OH and NO + H<sub>2</sub>O, are the dominant reaction channels. The rate constants for the various product channels calculated on the basis of our theoretical transition-

state energies and geometries are provided here for practical applications.

## Ab Initio Computation Methods

Geometries of the reactants, products, intermediates, and transition states (TS) have been optimized with the unrestricted Møller–Plesset second-order perturbation (UMP2)<sup>7</sup> method and Becke's three-parameter nonlocal exchange functional<sup>8</sup> with the nonlocal correlation functional of Lee, Yang, and Parr<sup>9</sup> (B3LYP) using the 6-311G(d,p) basis set.<sup>7</sup> Vibrational frequencies, also calculated at both levels of theory, have been used to characterize stationary points, zero-point energy (ZPE) corrections, and rate constant calculations. The number of imaginary frequencies for intermediates and transition states are 0 and 1, respectively. The ZPE and vibrational frequencies calculated at the B3LYP level of theory were used without scaling. However, the values calculated at the UMP2 level of theory were scaled by a factor of 0.95 for anharmonicity correction.<sup>7</sup> Furthermore, for comparison, geometry optimization for some transition states has also been carried out using the QCISD/6-311G(d,p)<sup>10</sup> method. To confirm that the transition states connect between designated intermediates, intrinsic reaction coordinate (IRC)<sup>11</sup> calculations were performed at the UMP2 and B3LYP levels of theory.

For the purpose of obtaining more reliable energies of various structures for rate constant calculation, a G2(PU) scheme<sup>12</sup> was performed for each species. The conventional G2 method<sup>5</sup> uses a series of calculations to approximate a QCISD(T)/6-311+G-(3df,2p) calculation with an additional "higher order correction" based on the number of paired and unpaired electrons. The G2(PU) scheme uses the MP2/6-311g(d,p) optimized geometries, scaled ZPE, and for the radical reactants and products, projected UMP4 and UMP2 (PUMP4 and PUMP2) energies, which give more reliable results for open-shell systems than the regular (unprojected) MP4 and MP2 methods.<sup>7</sup> For species

\* Corresponding author: e-mail address: chemmcl@emory.edu.

† Present address: Institute of Atomic and Molecular Sciences Academia Sinica, P.O. Box 23-166, Taipei 10764, Taiwan.

<sup>®</sup> Abstract published in *Advance ACS Abstracts*, December 1, 1996.

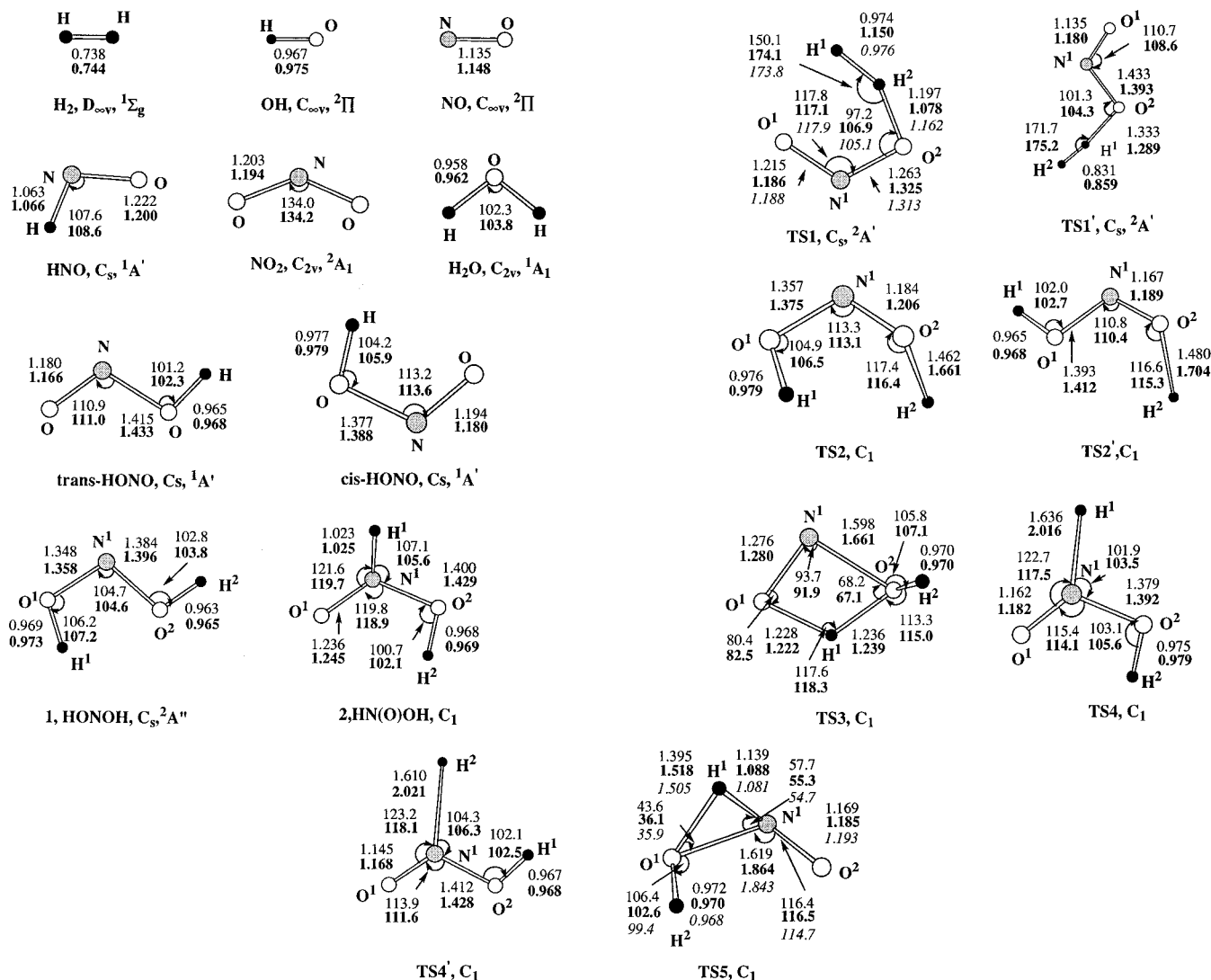


**Figure 1.** Optimized geometries (in Å and deg) of the reactants, products, intermediates, and transition states involved in the H + HONO reaction at the UMP2/6-311G(d,p) (plain numbers), the B3LYP/6-311G(d,p) (bold numbers) and the QCISD/6-311G(d,p) levels of theory (italic numbers).

optimized at the B3LYP/6-311G(d,p) and for two TSs at the QCISD/6-311G(d,p) levels of theory, we used the G2(PU) scheme to obtain their high-level energies, G2(PU//B3LYP) and G2(PU//QCISD), respectively, except the ZPE of G2(PU//QCISD), which was obtained by using the value calculated at the B3LYP level. All the calculations have been performed with the GAUSSIAN92/DFT program.<sup>13</sup>

The results obtained from these calculations are also compared with those from the BAC-MP4 method, which has been shown to give reliable data for many H/N/O systems.<sup>14</sup>

## Results and Discussion

**Potential Energy Surfaces and Reaction Mechanism.** The optimized geometries of the reactants, products, intermediates, and transition states for this reaction are shown in Figure 1. The values obtained by various methods are also given in the figure for comparison. The relative energies obtained at various levels of theory are collected in Table 1. The heats of formation of the reactants and products calculated at both levels of theory are presented in Table 2, and the vibrational frequencies and moments of inertia of all species in Tables 3 and 4. The potential energy surface drawn with the G2(PU//B3LYP) energies is shown in Figure 2.

There are three possible reaction mechanisms for the interaction of a hydrogen atom with cis-HONO, which is more reactive than its trans-isomer as will be shown later. The first one is

the commonly assumed direct hydrogen abstraction reaction, occurring by the attack of H at the hydrogen atom of HONO to produce H<sub>2</sub> + NO<sub>2</sub> through TS1. The barrier of TS1 calculated at the G2(PU//B3LYP) level is lower than that calculated at the G2(PU) level by 9.6 kcal/mol, but is in good agreement with that obtained at the BAC-MP4 level of theory. The difference in the energies between the G2(PU//B3LYP) and G2(PU) levels of theory is attributable to the large difference in their optimized geometries and ZPE. The optimized geometry of TS1 at the UMP2 level has a later transition-state character than that at the B3LYP level because TS1 at the UMP2 level has a longer O<sup>2</sup>H<sup>2</sup> distance and a shorter H<sup>1</sup>H<sup>2</sup> distance. The later character would result in a lower energy at the UMP2 level because this channel is an exothermic reaction. However, TS1 at the B3LYP level has larger ∠H<sup>1</sup>H<sup>2</sup>O<sup>2</sup> and ∠H<sup>2</sup>O<sup>2</sup>N<sup>1</sup> than those at the UMP2 level by 24.0° and 9.7°, respectively. The looser structure at the B3LYP level would result in a lower electronic energy. Furthermore, one can see from Table 1 that the ZPE at the B3LYP level is lower by 5.7 kcal/mol than that at the UMP2 level, because one of the TS1 frequencies by the latter method is higher than 4000 cm<sup>-1</sup> (Table 4). Obviously, this is an artifact of the UMP2 approximation, which is caused by spin contamination.<sup>15</sup> As discussed earlier,<sup>16</sup> the UMP2 method gives highly overestimated frequencies for some radicals, for example, NO. The B3LYP approach gives free radical frequencies that are in much better agreement with

**TABLE 1: Relative Energies (kcal/mol) and Zero-Point Energy Corrections (ZPE, kcal/mol) of Reactants, Products, Intermediates, and Transition States for the Reaction of H with HONO with the UMP2/6-311G(d,p), B3LYP/6-311G(d,p), and QCISD/6-311G(d,p) Optimized Geometries**

species	optimized at B3LYP/6-311G(d,p)				optimized at UMP2/6-311G(d,p)				G2 (PU// QCISD) <sup>d</sup>	BAC-MP4
	$\langle S^2 \rangle^a$	ZPE	B3LYP <sup>b</sup>	G2 (PU//B3LYP) <sup>b</sup>	$\langle S^2 \rangle^a$	ZPE <sup>c</sup>	UMP2 <sup>b</sup>	G2(PU) <sup>b</sup>		
H+cis-HONO	0.75, 0.0	12.7	0.0	0.0	0.75, 0.0	12.2	0.0	0.0	9.0	0.0
H+trans-HONO	0.75, 0.0	12.8	0.2	-0.6	0.75, 0.0	12.1	0.6	-0.7		1.4
NO+H <sub>2</sub> O	0.75, 0.0	16.2	-68.9	-68.0	0.78, 0.0	17.9	-68.0	-65.8		-69.6
HNO+OH	0.0, 0.75	13.9	0.6	1.8	0.0, 0.75	13.6	5.5	1.1		-0.5
H <sub>2</sub> +NO <sub>2</sub>	0.0, 0.75	11.9	-30.1	-25.3	0.0, 0.77	12.5	-26.5	-25.0		-26.3
HONOH, <b>1</b>	0.75	19.1	-42.8	-31.7	0.76	18.6	-30.6	-32.4		-36.0
HN(O)OH, <b>2</b>	0.75	19.9	-43.9	-29.7	0.77	19.6	-29.1	-29.9		-29.4
TS1	0.76	11.6	0.9	7.2	0.78	17.3	18.3	16.8		9.1
TS1'	0.76	10.8	9.3	16.9	0.81	14.1	22.1	22.0		15.4
TS2	0.77	13.5	3.8	10.1	0.98	13.8	27.8	12.5		10.3
TS2'	0.78	13.7	3.2	8.8	0.99	14.0	27.5	11.7	11.2	
TS3	0.75	16.0	-12.1	-2.6	0.77	16.3	-0.4	-2.2	-8.7	
TS4	0.77	13.4	1.0	4.9	0.94	14.5	15.6	7.9	5.3	
TS4'	0.77	13.5	1.1	4.2	0.96	14.7	16.9	7.7		
TS5	0.76	16.6	-15.9	-5.8	0.80	18.6	7.6	4.3	-1.2	-8.4

<sup>a</sup> The expectation value of  $\langle S^2 \rangle$  before projection. Values after projection are 0.75 for doublet states and 2.00 for triplet states. For reactants and products, the first number corresponds to the first species, and the second number corresponds to the second species. <sup>b</sup> The B3LYP/6-311G(d,p), G2(PU//B3LYP), UMP2/6-311G(d,p), and G2(PU) energies relative to the energies of H + cis-HONO. The energies of H + cis-HONO at B3LYP/6-311G(d,p), G2(PU//B3LYP), UMP2/6-311G(d,p), and G2(PU) levels are -206.264 31, -205.963 16, -205.775 07, and -205.962 71 hartrees, respectively. <sup>c</sup> Calculated at the UMP2/6-311G(d,p) level and scaled by 0.95. <sup>d</sup> G2(PU//QCISD) energy relative to the G2(PU//B3LYP) energy of H + cis-HONO.

**TABLE 2: Comparison of the Heats of Formation of the Reactants and Products from Experiment and from G2(PU), G2(PU//B3LYP), and BAC-MP4 Calculations**

kcal/mol	expt <sup>a</sup>	G2(PU)	G2(PU//B3LYP)	BAC-MP4
H	51.6	51.6	51.6	51.6
H <sub>2</sub>	0.	-0.9	-0.7	0.0
OH	9.2	9.3	9.3	9.5
H <sub>2</sub> O	-57.1	-57.0	-56.7	-57.1
HNO	24.5	24.5	25.0	24.1
NO	21.5	23.9	21.2	21.6
NO <sub>2</sub>	8.6	8.6	7.9	7.8
HONO(cis)	-16.9	-18.9	-19.1	-17.5
HONO(trans)	-17.4	-19.6	-19.7	-16.1

<sup>a</sup> Reference 23.

experiment than UMP2 does.<sup>17</sup> The dramatic difference in ZPE and the optimized geometries accounts for the 9.6 kcal/mol deviation at the two levels. Because of the large energy difference, a higher level calculation with QCISD/6-311G(d,p) was performed. The optimized geometry and G2(PU//QCISD) energy of TS1 are shown in Figure 1 and Table 1, respectively. The QCISD geometry of TS1 is between those obtained by the UMP2 and B3LYP. Because the ZPE of G2(PU//QCISD) was obtained from that of B3LYP, the G2(PU//QCISD) energy is closer to that of G2(PU//B3LYP).

The second possible mechanism occurs by the attachment of H to O<sup>2</sup> through TS2 to form HONOH, **1**, which has a C<sub>s</sub> symmetry and cis-trans HONO structure. The HONO reactant also has a C<sub>s</sub> symmetry; however, the attacking hydrogen atom in TS2 is out of the H<sup>1</sup>O<sup>1</sup>N<sup>1</sup>O<sup>2</sup> plane. No planar transition state for the addition of H to O<sup>2</sup> was found in our calculation. Furthermore, the IRC calculation starting from TS2 has shown that TS2 connects the reactants and species **1**. The nonplanar geometry of TS2 indicates that the approaching hydrogen atom forms a  $\sigma$  bond with a  $\pi$  electron instead of lone pair  $\sigma$  electrons of O<sup>2</sup>. **1** has a <sup>2</sup>A'' electronic state and five  $\pi$  electrons including two lone pairs on the oxygen atoms and an unpaired electron on the nitrogen. The HONO molecule has only four  $\pi$ -electrons, which include the lone pair on the O<sup>1</sup> atom and the  $\pi$  N-O electrons. During the time that the  $\pi$  bond is broken, a new O<sup>2</sup>-H<sup>2</sup> bond is formed and the lone pair of O<sup>2</sup> acquires a  $\pi$  character. The barrier of TS2 at the G2(PU//B3LYP) level of theory is lower than that at the G2(PU) level by 2.4 kcal; however, the former is in closer agreement with that of the BAC-

MP4 level of theory. The geometry of TS2 is quite sensitive to the methods used. For instance, the forming O<sup>2</sup>-H<sup>2</sup> bond changes from 1.462 Å at the UMP2 level to 1.661 Å at the B3LYP level. However, the G2(PU) energy is insensitive to the use of either the UMP2 or the B3LYP geometry. By this mechanism, the reaction proceeds with the elimination of H<sub>2</sub>O to produce the NO + H<sub>2</sub>O products through TS3, which is four-centered with energy lower than that of the reactants by ~2.5 kcal/mol at both the G2(PU) and G2(PU//B3LYP) levels of theory. Again, an IRC calculation was carried out for both backward and forward directions from TS3, leading to species **1** and NO + H<sub>2</sub>O, respectively.

The third possible reaction mechanism takes place by the attachment of H to the nitrogen atom of HONO through TS4 to form species **2**, HN(O)OH (hydroxyl nitroxide). The barrier for this addition reaction is 4.9, 7.9, and 5.3 kcal/mol at the G2(PU//B3LYP), G2(PU), and BAC-MP4 levels of theory, respectively. As in the case of TS2, the G2(PU//B3LYP) result agrees well with that of the BAC-MP4 method. The most apparent difference in geometric parameters predicted by UMP2 and B3LYP is the forming H<sup>1</sup>-N<sup>1</sup> bond, which increases from 1.636 Å with the former to 2.016 Å with the latter. Again, the B3LYP method gives a looser structure. The reaction proceeds with species **2** undergoing two possible fragmentation reactions: one gives NO + H<sub>2</sub>O through TS5, and the other gives HNO + OH without a clearly defined TS. The relative energy of TS5 to **2** calculated at the G2(PU) level of theory is different from that at the G2(PU//B3LYP) level of theory by as much as 10.1 kcal/mol and is different from that at the BAC-MP4 by 12.7 kcal/mol. The optimized geometry of the TS5 at the B3LYP level also has a looser structure than that obtained at the UMP2 level. For instance, the O<sup>1</sup>-N<sup>1</sup> and O<sup>1</sup>-H<sup>1</sup> distances optimized at the B3LYP level are longer than those optimized at the UMP2 level by 0.245 and 0.123 Å, respectively. Therefore, we also performed G2(PU//QCISD) calculations for this TS. The optimized geometry and G2(PU//QCISD) energy of TS5 are shown in Figure 1 and Table 1, respectively. The G2(PU//QCISD) energy is between those calculated by G2(PU) and G2(PU//B3LYP), and the QCISD geometry of TS 5 is closer to that of the B3LYP geometry.

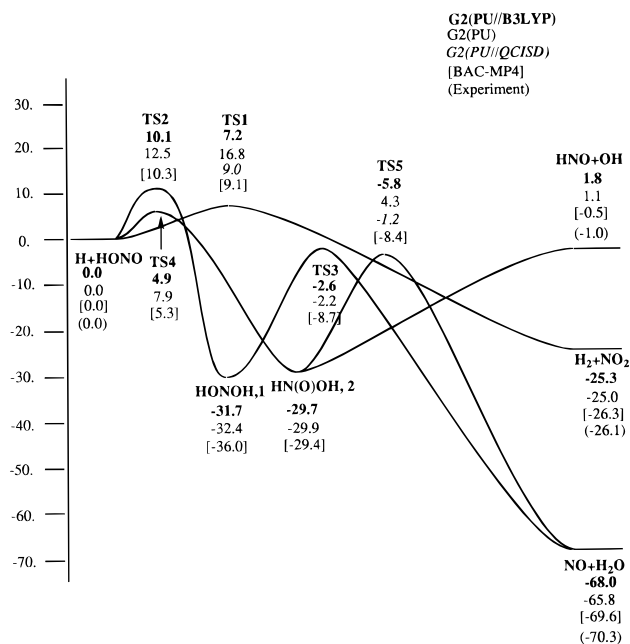
The calculations of the TSs for the addition of H to N<sup>1</sup> and O<sup>2</sup> of trans-H<sup>1</sup>O<sup>1</sup>N<sup>1</sup>O<sup>2</sup> and the abstraction of hydrogen from

**TABLE 3: Moments of Inertia (in au) and B3LYP/6-311G(d,p) Normal Vibrational Frequencies (in cm<sup>-1</sup>) for the Molecular Reactant, Intermediates, and Transition States of the Reaction of H and HONO**

species	I	$\omega_1$	$\omega_2$	$\omega_3$	$\omega_4$	$\omega_5$	$\omega_6$	$\omega_7$	$\omega_8$	$\omega_9$
cis-HONO	21.5, 135.0, 156.6	665	722	945	1338	1639	3656			
trans-HONO	19.2, 143.8, 163.0	609	620	834	1304	1793	3779			
HONON, <b>1</b>	29.7, 149.9, 179.6	205	345	575	970	1055	1323	1438	3671	3808
HN(O)OH, <b>2</b>	27.3, 157.0, 181.6	290	545	777	951	1300	1420	1524	3363	3753
TS1	38.2, 135.8, 174.1	255	315	761	982	1038	1372	1656	1721	951i <sup>a</sup>
TS1'	25.4, 164.2, 189.7	257	331	551	726	791	1024	1702	2164	1126i
TS2	32.8, 147.0, 169.8	196	502	652	689	921	1325	1555	3589	987i
TS2'	31.4, 151.6, 174.7	253	493	585	672	861	1298	1628	3770	918i
TS3	39.2, 144.5, 178.9	504	591	790	936	1260	1351	1985	3750	1911i
TS4	40.9, 141.9, 173.2	281	305	634	680	876	1337	1691	3594	525i
TS4'	38.8, 148.6, 178.9	279	300	593	623	828	1310	1764	3769	482i
TS5	27.2, 207.8, 230.3	340	493	679	885	1180	1671	2623	3746	1293i

<sup>a</sup> i denotes the imaginary frequency.**TABLE 4: Moments of Inertia (in au) and Scaled MP2/6-311G(d,p) Normal Vibrational Frequencies (in cm<sup>-1</sup>) for the Molecular Reactant, Intermediates, and Transition States of the Reaction of H and HONO**

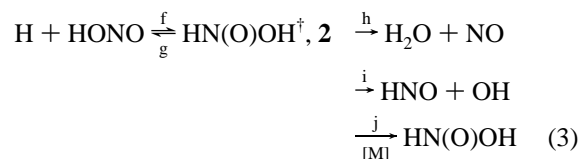
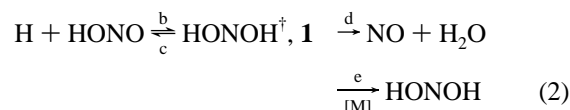
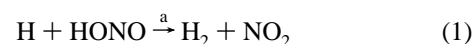
species	I	$\omega_1$	$\omega_2$	$\omega_3$	$\omega_4$	$\omega_5$	$\omega_6$	$\omega_7$	$\omega_8$	$\omega_9$
cis-HONO	21.5, 135.0, 156.6	632	686	898	1271	1557	3473			
trans-HONO	19.3, 142.7, 162.0	576	606	821	1243	1603	3650			
HONOH, <b>1</b>	29.2, 147.4, 176.7	181	328	569	976	1058	1282	1390	3572	3689
HN(O)OH, <b>2</b>	26.6, 153.1, 177.9	306	537	786	948	1285	1398	1561	3288	3619
TS1	32.2, 130.2, 162.4	539	816	957	1182	1244	1373	1763	4211	1493i <sup>a</sup>
TS1'	26.2, 164.9, 191.1	168	340	591	601	737	907	2406	4102	1793i
TS2	29.5, 142.5, 163.5	266	583	654	757	935	1306	1648	3485	2380i
TS2'	27.8, 147.5, 168.1	323	536	625	744	875	1276	1718	3657	2398i
TS3	37.4, 140.3, 172.7	485	781	897	1048	1233	1390	1949	3597	1675i
TS4	34.1, 138.4, 166.9	511	549	617	695	856	1304	2145	3498	1698i
TS4'	31.1, 145.9, 172.3	459	567	602	659	812	1275	2289	3628	1682i
TS5	25.9, 172.8, 193.9	410	561	966	1157	1723	1996	2653	3568	1986i

<sup>a</sup> i denotes the imaginary frequency.**Figure 2.** Potential energy profile for the H + HONO reaction at G2-(PU) (plain numbers), G2(PU//B3LYP) (bold numbers), G2(PU//QCISD) (bold numbers in italics), and BAC-MP4 (numbers in brackets) and experimental values (numbers in parentheses). The curves are drawn with the G2(PU//B3LYP) results.

the trans-structure were also carried out. The geometries and relative energies are shown in Figure 1 and Table 1, respectively. The barrier for hydrogen abstraction from the trans-isomer is higher than that from the cis-isomer by at least 4.9 kcal/mol among the three levels of theory. The cis-isomer is apparently more reactive, as has been concluded in our recent study of the NH<sub>2</sub> + HONO reaction.<sup>18</sup> On the other hand, the difference in the barriers for the addition of H to N and O atoms of the cis-

and trans-structures is less than 0.5 kcal/mol. Since the cis-trans isomerization occurs readily above room temperature, our rate constant calculations were carried out only for cis-HONO reactions.

The three reaction mechanisms presented above can be summarized as follows:



where “<sup>†</sup>” stands for internal excitation.

**Rate Constant Calculation.** A. *Conventional Transition-State Calculation of the Rate Constant for Mechanism 1.* Reaction a occurs by the direct hydrogen abstraction mechanism without involving a long-lived complex. Therefore, the rate constant for this reaction can be computed with the conventional transition-state theory (CTST). The calculation was based on the energy barrier obtained by G2(PU//QCISD), which is the highest level of theory among the three employed. According to the general TST, rate constant  $k$  at temperature  $T$  can be expressed as<sup>19</sup>

$$k(T) = \alpha \frac{k_B T}{h} \exp\left(\frac{-\Delta G^\ddagger(T)}{k_B T}\right)$$

Here  $\alpha$  is the statistical factor (the number of equivalent reaction

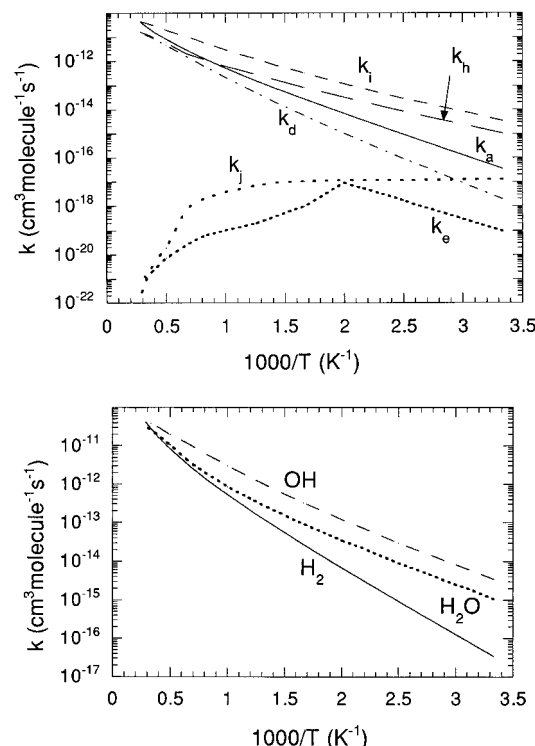


**Figure 3.** (a, top) Arrhenius plots of the rate constants from a TST calculation for step a and RRKM calculations for steps d, e, h, i, and j at 760 Torr. (b, bottom) Arrhenius plot of the rate constants for the formation of OH, H<sub>2</sub>, and H<sub>2</sub>O products.

**TABLE 5: Maximum  $\Delta G^\ddagger$ , the Corresponding NO<sup>+</sup> Distance, and the Rate Constant for Unimolecular Decomposition of HN(O)OH, HN(O)OH  $\rightarrow$  HNO + OH, Calculated on the Basis of Canonical Variational Transition-State Theory**

T, K	NO <sup>+</sup> , Å	$\Delta G^\ddagger$ , kcal/mol <sup>a</sup>	$k$ , s <sup>-1</sup>
300	2.42	29.83	$1.15 \times 10^{-9}$
400	2.39	29.24	$8.77 \times 10^{-4}$
500	2.36	28.65	3.11
600	2.35	28.07	$7.43 \times 10^2$
700	2.33	27.52	$3.71 \times 10^4$
800	2.31	26.98	$7.08 \times 10^5$
1000	2.29	26.01	$4.30 \times 10^7$
1200	2.27	25.11	$6.66 \times 10^8$
1500	2.24	23.75	$1.08 \times 10^{10}$
2000	2.01	23.22	$1.21 \times 10^{11}$
2500	1.98	23.01	$5.06 \times 10^{11}$
3000	1.95	23.13	$1.29 \times 10^{12}$
3500	1.93	23.42	$2.51 \times 10^{12}$

<sup>a</sup> Calculated at the CCSD(T)/6-311G(d,p) level, relative to HN(O)OH. Standard states: 1 bar of ideal gas. See Appendix A for geometric data.

channels);  $k_B$  is the Boltzmann constant;  $h$  is Planck's constant; and  $\Delta G^\ddagger(T)$  is the standard-state free energy of activation. The Arrhenius plot for  $k_a$  is shown in Figure 3. A least-squares analysis of the calculated  $k_a$  values gives

$$k_a = 3.33 \times 10^{-16} T^{1.55} \exp(-3328.5/T) \text{ cm}^3 \text{ molecule}^{-1} \text{ s}^{-1}$$

over the temperature range 300–3500 K.

**B. RRKM Calculations of Rate Constants for Mechanisms 2 and 3.** For the second and third reaction mechanisms, there is no dramatic difference between G2(PU) and G2(PU//B3LYP) energies except for TS5. For rate constant calculations, therefore, we have chosen the G2(PU//QCISD) energy for TS5 and G2(PU//B3LYP) energies for the other species.

Since both reaction mechanisms involve the formation of long-lived complexes, RRKM calculations were carried out for

**TABLE 6: Calculated Rate Constants (cm<sup>3</sup> molecule<sup>-1</sup> s<sup>-1</sup>) for the H + cis-HONO Association–Decomposition Reaction at Various Temperatures and Pressures**

T	100 Torr			760 Torr			200 atm		
	$k_d + k_h$	$k_e$	$k_i$	$k_j$	$k_d + k_h$	$k_e$	$k_i$	$k_j$	$k_e$
500	$3.47 \times 10^{-14}$	$7.14 \times 10^{-21}$	$1.20 \times 10^{-13}$	$2.20 \times 10^{-19}$	$3.48 \times 10^{-14}$	$8.99 \times 10^{-18}$	$1.20 \times 10^{-13}$	$1.10 \times 10^{-17}$	$9.12 \times 10^{-16}$
1000	$8.54 \times 10^{-13}$	$3.16 \times 10^{-22}$	$3.02 \times 10^{-12}$	$9.19 \times 10^{-20}$	$8.54 \times 10^{-13}$	$1.01 \times 10^{-19}$	$3.02 \times 10^{-12}$	$3.66 \times 10^{-18}$	$1.24 \times 10^{-13}$
1500	$3.78 \times 10^{-12}$	$1.11 \times 10^{-22}$	$1.10 \times 10^{-11}$	$2.17 \times 10^{-20}$	$3.78 \times 10^{-12}$	$2.56 \times 10^{-20}$	$1.10 \times 10^{-11}$	$7.65 \times 10^{-19}$	$2.77 \times 10^{-13}$
2000	$1.05 \times 10^{-11}$	$3.74 \times 10^{-23}$	$1.97 \times 10^{-11}$	$1.37 \times 10^{-21}$	$1.05 \times 10^{-11}$	$7.55 \times 10^{-21}$	$1.97 \times 10^{-11}$	$1.87 \times 10^{-21}$	$1.08 \times 10^{-13}$
3000	$2.60 \times 10^{-11}$	$6.52 \times 10^{-24}$	$3.88 \times 10^{-11}$	$3.51 \times 10^{-23}$	$2.60 \times 10^{-11}$	$1.09 \times 10^{-21}$	$3.88 \times 10^{-11}$	$8.64 \times 10^{-22}$	$1.26 \times 10^{-14}$

the total and individual step rate constants by solving individual master equations.<sup>20</sup> The procedure for such calculations has been discussed in our previous papers.<sup>20,21</sup> The molecular parameters for the calculations are summarized in Table 3. The dissociation process (i) does not have a well-defined TS because of the absence of reaction barrier for its reverse process. To circumvent the difficulty, we applied the canonical variational method based on the maximum value of free energy,  $\Delta G^\ddagger$ , computed at each temperature along the reaction coordinate, as also discussed in our previous paper on  $\text{HCO} + \text{O}_2$ .<sup>21</sup> To find  $\Delta G^\ddagger$  for each temperature, we first scanned the potential energy surface for the dissociation into  $\text{OH} + \text{HNO}$ . The dissociating NO distance was varied from 1.8 to 2.5 Å at intervals of 0.1 Å; other geometric parameters were optimized for each value of N–O. Therefore, we calculated eight optimized geometries for the various NO distances from 1.8 to 2.5 Å. For each structure, we calculated the  $3N-7$  vibrational frequencies, projected out of the gradient direction. To obtain more reliable energies, we also performed CCSD(T) calculations for the individually optimized geometries. Furthermore, we used a Morse potential to fit the potential energies calculated at the CCSD(T) level.

The resulting potential energy function  $E(R)$  is given by

$$E(R) = D_e[1 - e^{-\beta(R-R_e)}]^2$$

where  $R_e = 1.429$  Å is the equilibrium value of  $R$ , i.e., the equilibrium N–O bond distance of species **2**; the parameter  $\beta$  was determined to be  $4.2 \text{ Å}^{-1}$  by fitting our CCSD(T) energies; and  $D_e$  is the dissociating energy, 32.0 kcal/mol, obtained at the CCSD(T) level, excluding ZPE. The Morse potential energy, computed moments of inertia, and vibrational frequencies shown in Appendix A were used for the calculation of  $\Delta G$ . We looked for the maximum values of  $\Delta G$  at various temperatures in the range 300–3500 K. The accurate position of the maximum free energy for each temperature, calculated on the basis of the parabolic fit of the three largest  $\Delta G$  values, is shown in Table 5. Using the maximum  $\Delta G^\ddagger$ , we calculated the VTST rate constant for the  $\text{HN(O)OH} \rightarrow \text{HNO} + \text{OH}$  dissociation, also shown in Table 5. The rate constant is fitted to give the following expression for the dissociation process:

$$k_{(2 \rightarrow \text{HNO} + \text{OH})} = 3.83 \times 10^{14} \exp(-16750/T) \text{ s}^{-1}$$

In the RRKM calculation, we used for the transition state of step i the molecular parameters of the structure with maximum  $\Delta G^\ddagger$  at each temperature. As the maxima are located between the calculated structures, the corresponding moments of inertia and vibrational frequencies were linearly interpolated.

The results of RRKM calculations for the second and third reaction mechanisms are shown in Figure 3a in comparison with that of reaction a. The overall rate constant for the formation of OH,  $\text{H}_2\text{O}$ , and  $\text{H}_2$  is individually shown in Figure 3b. The bimolecular rate constants for the H + HONO reactions occurring via steps d, h, and i are fitted by least-squares and given in units of  $\text{cm}^3 \text{ molecule}^{-1} \text{ s}^{-1}$  as follows:

$$k_d = 1.71 \times 10^{-14} T^{1.02} \exp(-4504.2/T)$$

$$k_h = 1.72 \times 10^{-16} T^{1.49} \exp(-1995.9/T)$$

$$k_i = 9.36 \times 10^{-14} T^{0.86} \exp(-2500.8/T)$$

for the temperature range 300–3500 K. In the second and third reaction mechanisms, the deactivation processes, e and f, under atmospheric pressure conditions are so small that they can be neglected. At low temperatures, the formation of  $\text{H}_2\text{O}$  and OH by processes h and i, respectively, are the dominant channels.

At temperatures above 2000 K, all three channels, including the direct hydrogen abstraction reaction a, are competitive. For practical applications, we have also listed in Table 6 the individual rate constants for production of OH ( $k_i$ ),  $\text{H}_2\text{O}$  ( $k_d + k_h$ ),  $\text{N(OH)}_2$  ( $k_e$ ), and  $\text{HN(O)OH}$  ( $k_j$ ) as functions of temperature and pressure.

## Concluding Remarks

According to the results of ab initio calculations, the H + HONO reaction can take place by three different mechanisms. The first mechanism involves direct hydrogen abstraction via TS1 to produce  $\text{H}_2 + \text{NO}_2$ , and the barrier calculated at our best G2(PU//QCISD) level is 9.0 kcal/mol. The second mechanism occurs by hydrogen addition to the terminal oxygen of HONO to give the excited  $\text{HONO}^* (\mathbf{1})$ , which can proceed by further eliminating  $\text{H}_2\text{O}$  exothermally. The rate-determining step is hydrogen addition with a barrier at TS2 somewhat higher than that for hydrogen abstraction. The third mechanism involves hydrogen addition to the nitrogen atom of HONO with the formation of the excited  $\text{HN(O)OH}^* (\mathbf{2})$  followed by either  $\text{H}_2\text{O}$  or OH elimination. The hydrogen addition step with TS4 is rate-controlling. The barrier to TS4 is found to be lower by 4–5 kcal/mol than the barriers for the  $\text{H} + \text{HONO} \rightarrow \text{H}_2 + \text{NO}_2$  and  $\text{H} + \text{HONO} \rightarrow \text{HONO}^* (\mathbf{1})$  mechanisms.

The rate constants for all reaction mechanisms have been calculated using TST and RRKM approaches. The results show that the direct hydrogen abstraction is the least important channel in temperatures lower than 2000 K, whereas the H-for-OH indirect displacement dominates the reaction, and the formation of  $\text{H}_2\text{O} + \text{NO}$  is the next key product channel.

**Acknowledgment.** The authors gratefully acknowledge the support of this work by the Office of Naval Research (Contract No. N00014-89-J-1949) under the direction of Dr. R. S. Miller. We are also obliged to the Cherry L. Emerson Center for Scientific Computations for the use of various programs and computing facilities.

## Appendix A

**TABLE 7: Energies and Molecular Parameters for the  $\text{HN(O)OH}$  Structures Optimized at Various NO Distances**

$R(\text{N-O}), \text{Å}$	$E_{\text{rel}}^a (\text{kcal/mol})$	$i$	$I_i$ (atomic units)	$\nu_j (\text{cm}^{-1})$
1.8	19.91	A	29.0	233, 430, 830
		B	206.6	1096, 1266, 1562,
		C	230.3	3251, 3776
1.9	23.72	A	29.0	229, 385, 774,
		B	223.6	1021, 1240, 1589,
		C	246.9	3206, 3775
2.0	26.41	A	28.8	213, 333, 691,
		B	242.9	924, 1266, 1606,
		C	265.4	3155, 3770
2.1	28.25	A	28.6	162, 280, 594,
		B	263.6	820, 1306, 1610,
		C	285.1	3108, 3763
2.2	29.49	A	28.3	165, 236, 517,
		B	285.8	735, 1335, 1608,
		C	305.8	3071, 3761
2.3	30.32	A	28.0	189, 199, 449,
		B	308.4	651, 1359, 1604,,
		C	327.8	3038, 3757
2.4	30.88	A	27.7	158, 169, 386,
		B	332.2	570, 1380, 1597,
		C	351.0	3010, 3749
2.5	31.24	A	27.3	79, 144, 312,
		B	356.7	486, 1399, 1591,
		C	374.6	2985, 3742

<sup>a</sup> Energy relative to  $\text{HN(O)OH}$  at the CCSD(T) level of theory, based on the fitted Morse potential.

## References and Notes

- (1) Kuo, K. K.; Summerfield, M. *Fundamentals of Solid-Propellant Combustion*; AIAA, Inc.: New York, 1984.
- (2) Atkinson, R.; Baulch, D. L.; Cox, R. A.; Hampson, R. F., Jr.; Kerr, J. A.; Troe, J. *J. Phys. Chem. Ref. Data* **1992**, *21*, 1125.
- (3) Kerr, J. A. In *Handbook of Physics and Chemistry*; Weast, R. C., Ed.; CRC Press: Boca Raton, FL, 1988–89; pp F-184.
- (4) Tsang, W.; Herron, J. T. *J. Phys. Chem. Ref. Data* **1991**, *20*, 609.
- (5) Curtiss, L. A.; Raghavachari, K.; Trucks, G. W.; Pople, J. A. *J. Chem. Phys.* **1991**, *94*, 7221.
- (6) Melius, C. F.; Binkley, J. S. *20th Symp. (Int.) Combust., [Proc.]* **1984**, 575.
- (7) For the description of the UMP2 method and basis sets, see: Hehre, W.; Radom, L.; Schleyer, P. v. R.; Pople, J. A. *Ab Initio Molecular Orbital Theory*; Wiley: New York, 1986.
- (8) (a) Becke, A. D. *J. Chem. Phys.* **1993**, *98*, 5648. (b) Becke, A. D. *J. Chem. Phys.* **1992**, *96*, 2155.
- (9) Lee, C.; Yang, W.; Parr, R. G. *Phys. Rev.* **1988**, *B37*, 785–789.
- (10) Pople, J. A.; Head-Gordon, M.; Raghavachari, K. *J. Chem. Phys.* **1987**, *87*, 5768.
- (11) Gonzalez, C.; Schlegel, H. B. *J. Phys. Chem.* **1989**, *90*, 2154.
- (12) (a) Mebel, A. M.; Morokuma, K.; Lin, M. C. *J. Chem. Phys.* **1994**, *101*, 3916. (b) Mebel, A. M.; Morokuma, K.; Lin, M. C.; Melius, C. F. *J. Phys. Chem.* **1995**, *99*, 1900.
- (13) Frisch, M. J.; Trucks, G. W.; Head-Gordon, M.; Gill, P. M. W.; Wong, M. W.; Foresman, J. B.; Johnson, B. G.; Schlegel, H. B.; Robb, M. A.; Replogle, E. S.; Gomperts, R.; Andres, J. L.; Raghavachari, K.; Binkley, J. S.; Gonzalez, C.; Martin, R. L.; Fox, D. J.; Defrees, D. J.; Baker, J.; Stewart, J. J. P.; Pople, J. A. *GAUSSIAN 92/DFT*; Gaussian, Inc.: Pittsburgh, PA, 1993.
- (14) (a) Mebel, A. M.; Morokuma, K.; Lin, M. C.; Melius, C. F. *J. Phys. Chem.* **1995**, *99*, 1900. (b) Diau, E. W. G.; Lin, M. C.; He, Y.; Melius, C. F. *Prog. Energy Combust. Sci.* **1995**, *1*, 21.
- (15) Jensen, F. *Chem. Phys. Lett.* **1990**, *169*, 519.
- (16) Mebel, A. M.; Morokuma, K.; Lin, M. C. *J. Chem. Phys.* **1994**, *101*, 3916.
- (17) Mebel, A. M.; Morokuma, K.; Lin, M. C. *J. Chem. Phys.* **1995**, *103*, 7414.
- (18) Mebel, A. M.; Diau, E. W. G.; Lin, M. C.; Morokuma, K. *J. Phys. Chem.* **1996**, *100*, 7517.
- (19) Laidler, K. J. *Chemical Kinetics*, 3rd ed.; Harper and Row: New York, 1987; p 124.
- (20) Diau, E. W. G.; Lin, M. C. *J. Phys. Chem.* **1995**, *99*, 6589.
- (21) Hsu, C.-C.; Mebel, A. M.; Lin, M. C. *J. Chem. Phys.* **1996**, *105*, 2346.
- (22) Mebel, A. M.; Morokuma, K. *J. Phys. Chem.* **1996**, *100*, 2985.
- (23) Chase, M. W., Jr.; Davies, C. A.; Downey, J. R., Jr.; Frurip, D. J.; McDonald, R. A.; Syverud, A. N. JANAF Thermochemical Tables, *J. Phys. Chem. Ref. Data* **1985**, *14*, Suppl. 1.